

Chemical Science

Accepted Manuscript



This is an *Accepted Manuscript*, which has been through the Royal Society of Chemistry peer review process and has been accepted for publication.

Accepted Manuscripts are published online shortly after acceptance, before technical editing, formatting and proof reading. Using this free service, authors can make their results available to the community, in citable form, before we publish the edited article. We will replace this *Accepted Manuscript* with the edited and formatted *Advance Article* as soon as it is available.

You can find more information about *Accepted Manuscripts* in the [Information for Authors](#).

Please note that technical editing may introduce minor changes to the text and/or graphics, which may alter content. The journal's standard [Terms & Conditions](#) and the [Ethical guidelines](#) still apply. In no event shall the Royal Society of Chemistry be held responsible for any errors or omissions in this *Accepted Manuscript* or any consequences arising from the use of any information it contains.



Journal Name

ARTICLE

A Cell-Penetrating Protein Designed for Bimodal Fluorescence and Magnetic Resonance Imaging

Qin Wu,^{a†} Qinqin Cheng,^{a†} Siming Yuan,^a Junchao Qian,^b Kai Zhong,^b Yinfeng Qian^c and Yangzhong Liu^{a*}

Received 00th January 20xx,
Accepted 00th January 20xx

DOI: 10.1039/x0xx00000x

www.rsc.org/

Multimodal imaging is a highly desirable biomedical application since it can provide complementary information from each imaging modality. We propose a protein engineering-based strategy for the construction of a bimodal probe for fluorescence and magnetic resonance imaging. A recombinant protein was generated by fusion of supercharged green fluorescence protein (GFP³⁶⁺) with a lanthanide-binding tag (dLBT) that can stably bind two Gd³⁺ ions. The GFP³⁶⁺-dLBT fusion protein showed strong fluorescence and exhibited efficient contrast enhancement in magnetic resonance imaging. This protein probe improves the MR relaxation more efficiently than the Gd-DTPA (gadopentetate dimeglumine). The superior cell-penetrating activity of GFP³⁶⁺ allows efficient cellular uptake of this fusion protein and can thus be used as a cellular imaging probe. Dual imaging was conducted *in vitro* and in mice. This result indicates that the fusion of different functional domains is a feasible approach for making multi-modal imaging agents.

Introduction

Over the past decades, a variety of molecular imaging techniques, such as positron emission tomography (PET), X-ray computed tomography (CT), magnetic resonance imaging (MRI) and fluorescence imaging (FI), have found numerous useful applications.^{1, 2} Each method has its inherent advantages and limitations. Therefore a single imaging method may not meet all of the requirements to solve a particular diagnostic problem.³ A combination of different imaging methods may achieve multi-modal imaging and facilitate bench-to-clinical applications.^{4, 5} A typical example is the probe that combines fluorescence and magnetic resonance imaging.^{6, 7} These two imaging modalities are highly complementary so that hybrid probes can exploit both the sensitivity of FI and resolution and deep tissue penetration of MRI.⁸⁻¹⁰

The synthesis of bimodal FI/MRI imaging probes is typically based on the chemical conjugation of two distinct functional modalities, such as organic molecules and inorganic nanoparticles.^{6, 11, 12} Although the chemical syntheses of bimodal probes have been investigated intensively, complex synthetic procedures are often required, thus limiting the

general applicability of this strategy. Biological properties of these products, such as toxicity, are hard to predict. A lack of chemical stability and a property such as photobleaching are other possible complications.¹³⁻¹⁵

Although biocompatible molecules such as proteins have been used to prepare multi-modal imaging agents, chemical modification is by far the most common approach to link a particular functional group to a protein of interest.^{16, 17} The introduction of various chemical substituents could limit further applications since only certain types of chemical modification are compatible with the clinical use of such proteins.¹⁸

To address these challenges, we developed an alternative strategy for obtaining a bimodal FI/MRI imaging probe, based solely on a protein engineering approach. Fusion proteins often retain the functional properties of the individual domains that comprise the fusion. Functional fusion proteins with MRI and FI modalities could serve as dual-imaging probes



Scheme 1. Cartoon representation of a bimodal imaging probe of a GFP³⁶⁺-dLBT fusion protein. Two gadolinium ions bound to dLBT are shown as pink spheres.

^aCAS Key Laboratory of Soft Matter Chemistry, CAS High Magnetic Field Laboratory, Department of Chemistry, University of Science and Technology of China, Hefei, 230026, Anhui, China.

^bHigh Magnetic Field Laboratory, Chinese Academy of Sciences, Hefei, 230031, China.

^cRadiology Department, the First Affiliated Hospital of Anhui Medical University, Hefei, 230022, China

† These authors contributed equally to this work.

Electronic Supplementary Information (ESI) available: [details of any supplementary information available should be included here]. See DOI: 10.1039/x0xx00000x

without the need for any further chemical modification. As a proof-of-concept, a GFP³⁶⁺-dLBT protein was generated by fusion of supercharged green fluorescence protein (GFP³⁶⁺) and a double-lanthanide-binding tag (dLBT), using standard protein expression procedures (Scheme 1). The dual imaging of this protein probe was tested *in vitro*, in cells and in mice. Results confirmed that the fusion of protein with different functional domains is a feasible approach for making multimodal imaging probes.

Results and discussion

Preparation and characterization

GFP³⁶⁺ is a variant of green fluorescence protein with 36 positive charges (also termed +36GFP).¹⁹ This supercharged GFP protein is highly aggregation-resistant and retains its fluorescence even after having been boiled or cooled.¹⁹ It shows superior cell-penetrating activity and for that reason it was used as a protein carrier for the delivery of siRNA into cells.²⁰ dLBT is an artificially designed peptide tag with high affinity for lanthanide ions.²¹ The peptide sequence of dLBT has been optimized for MRI purposes by the introduction of an H₂O coordination site to Gd³⁺ in the Gd-dLBTs complexes.²² This peptide can be fused to proteins with retention of Gd³⁺ binding ability.²² The cell-penetration property of the supercharged GFP³⁶⁺ domain allows cellular imaging of this fusion protein. To the best of our knowledge, this is the first bimodal FI/MRI agent made using an entirely genetically encoded protein.

The GFP³⁶⁺-dLBT fusion protein was obtained by expression in *E. coli* and purified by standard methods. (see Experimental Section for more details). To improve its stability, a flexible glycine-serine linker was inserted between GFP³⁶⁺ and dLBT.²³ (Scheme 1) After comparing different lengths of the linker, (GGG)₉ was chosen for further investigation, as this linker results in a stable fusion protein with appropriate MR imaging properties (Figure S2).

In vitro characterization

To explore whether the fusion protein retains the functionality of the two individual domains, fluorescence and metal binding properties of GFP³⁶⁺-dLBT were analyzed *in vitro*. Inductively coupled plasma mass spectroscopy (ICP-MS) measurements showed the fusion protein bound two Gd³⁺ ions (Figure 1A, Table S1). The number of gadolinium ions in the protein is consistent with the design of the fusion protein.²² No gadolinium was detected in the GFP³⁶⁺ protein, suggesting the presence of (His)₆ tag does not alter the binding of Gd³⁺ ions to the protein. UV titration showed that the binding constant of GFP³⁶⁺-dLBT fusion protein (K_d=114 nM) is comparable to literature data of other LBT variants (Figure S3).²² Fluorescence measurements showed nearly identical spectra of Gd(III) bound GFP³⁶⁺-dLBT fusion protein in comparison to the GFP³⁶⁺

protein (Figure 1B), indicating the fluorescence quantum yield of GFP protein is not perturbed by the fusion of dLBT and the Gd(III) binding. Thus, the fusion protein retains the functions of fluorescence and gadolinium binding, hence is suitable for optical and MRI bimodal imaging.

We next measured relaxivity and MR contrast enhancement of the fusion protein. A contrast agent used clinically, gadopentetate dimeglumine (Gd-DTPA) was used for comparison. Gd-GFP³⁶⁺-dLBT complex clearly exhibits the MR contrast enhancement, whereas no detectable signal was observed in the GFP³⁶⁺ protein without fusion of dLBT (Figure S3). This observation confirms the binding of Gd³⁺ ions to the dLBT domain. Imaging by MRI showed increasing contrast with the concentration of Gd-GFP³⁶⁺-dLBT (Figure 1C). The longitudinal relaxation rate (r_1) was measured at different gadolinium concentrations. Fitting the data gave a T₁ relaxivity 5.1 mM⁻¹s⁻¹ (Figure 1C). This value is greater than that of Gd-DTPA (3.67 mM⁻¹s⁻¹) under the same conditions (Figure S5). The GFP³⁶⁺-dLBT protein can thus serve as an efficient T₁ contrast agent. The greater relaxivity enhancement of GFP³⁶⁺-dLBT should in all likelihood be attributed primarily to the reduced rotational correlation of the protein in comparison to the small molecule contrast agent Gd-DTPA.²⁴

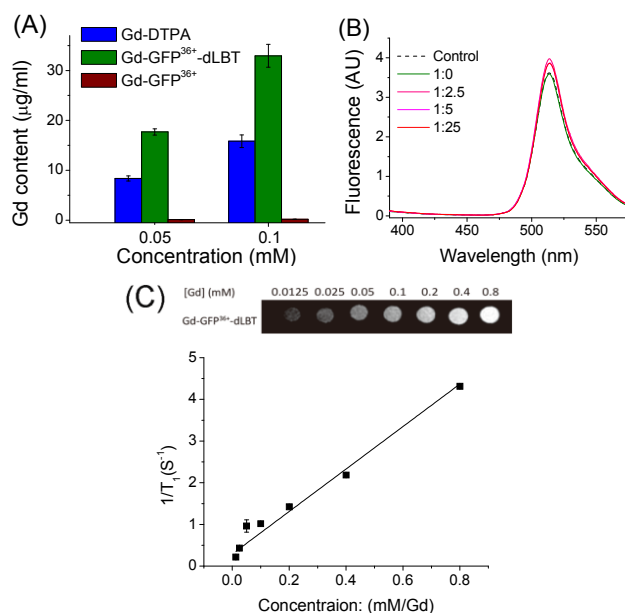


Figure 1. *In vitro* characterization of GFP³⁶⁺-dLBT protein. (A) ICP-MS measurement of Gd(III) content in Gd-DTPA (blue), Gd-GFP³⁶⁺-dLBT (green) and Gd-GFP³⁶⁺ (brown). Both GFP³⁶⁺-dLBT and GFP³⁶⁺ proteins contain a (His)₆ tag. (B) Fluorescence spectra of GFP³⁶⁺-dLBT with Gd³⁺ titration. The dashed line denotes the GFP³⁶⁺ control; the solid lines indicate the 10 µM GFP³⁶⁺-dLBT with the addition of Gd³⁺ ions. Molar ratios of [protein]:[Gd³⁺] are given. The spectra were recorded in HEPES buffer from 400–580 nm with an excitation wavelength of 395 nm. (C) T₁-weighted MR image produced with a spin echo sequence (TR 300 ms, TE 14 ms) of the GFP³⁶⁺-dLBT protein at different concentrations of gadolinium. The molar relaxivity rates r_1 ($1/T_1$) were obtained by linear fitting experimental data. Error bars denote standard deviation.

Dual imaging in cells

Since the GFP³⁶⁺ protein also possesses the unique feature of being able to penetrate cells, the dual imaging capability of GFP³⁶⁺-dLBT was tested. Cells were analyzed using confocal laser microscopy after treatment with Gd-GFP³⁶⁺-dLBT for four hours. Cytoplasmic fluorescence clearly showed internalization of GFP³⁶⁺-dLBT in cells (Figure 2A). Flow cytometry showed that cellular uptake of GFP³⁶⁺-dLBT increased rapidly with

increasing protein concentration (Figure S6). We also measured uptake of Gd-GFP³⁶⁺-dLBT by quantification of Gd ions in cells. The intracellular concentration of Gd increased with the concentration of Gd-GFP³⁶⁺-dLBT (Figure 2B). This result confirmed that Gd ions are internalized together with Gd-GFP³⁶⁺-dLBT, suggesting the possible application of this protein in the cellular MR imaging.

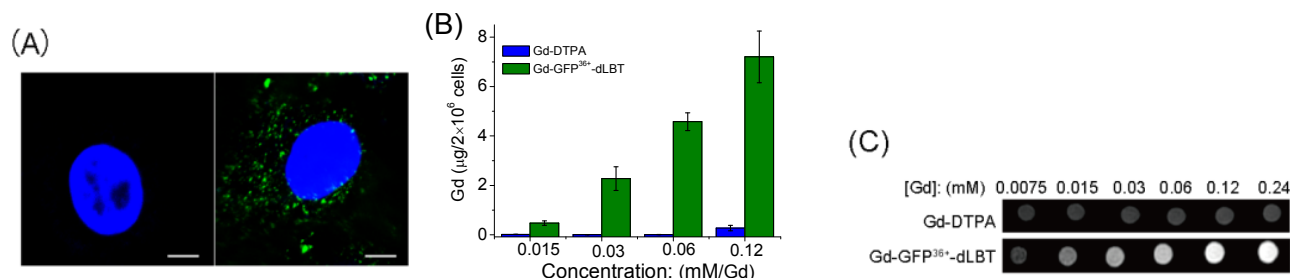


Figure 2. Cellular imaging of Gd-GFP³⁶⁺-dLBT. (A) Confocal laser microscopy images of HeLa cells treated with PBS (left) or 1 μM Gd-GFP³⁶⁺-dLBT (right) for 4 h. In blue: nuclear staining (DAPI), in green: GFP³⁶⁺. The scale bar is 15 μm. (B) Gd content in HeLa cells measured using ICP-MS after incubation with Gd-DTPA or Gd-GFP³⁶⁺-dLBT for 4 h. Data are shown as the mean ± SD of three independent experiments. (C) T₁-weighted MR images of 2 × 10⁶ HeLa cells treated with Gd-DTPA or Gd-GFP³⁶⁺-dLBT at different concentrations. Cells were washed 5 times to remove the free protein.

The T₁-weighted MR image was measured on HeLa cells treated with Gd-GFP³⁶⁺-dLBT. Enhanced signal strength was concentration-dependent (Figure 2C). Application of Gd-DTPA showed no such MR enhancement, in line with expectations, since Gd-DTPA is an extracellular contrast agent incapable of entering cells.²⁵ Similar results were observed on HepG2 cells (Figure S7). The different protein concentrations used in the fluorescence and MRI assays are corresponding to the sensitivity of two imaging methods.

Dual imaging in vivo

The *in vivo* imaging capabilities of Gd-GFP³⁶⁺-dLBT were investigated in tumor-bearing mice. The HepG2 tumor was implanted by injection into the flank above the upper left thigh. After tumor growth to an appropriate size, Gd-GFP³⁶⁺-dLBT was injected intratumorally followed by *in vivo* imaging. Fluorescence images were obtained before (0 h) and after injection (3 h) using a whole body imaging system. The images show fluorescence at the site of injection (dashed circle and arrow) (Figure 3A). After fluorescence imaging, the complementary MRI contrast efficiency was measured at the same time points using a 9.4 T MRI scanner. The T₁-weighted MR images also showed contrast enhancement at the site of injection (Figure 3B). In comparison with fluorescence imaging, MRI showed higher resolution and more accurately revealed the location and distribution of the injected Gd-GFP³⁶⁺-dLBT. This difference is in line with expectations based on the distinctive features of the two imaging methods.²⁶ Gd-GFP³⁶⁺-dLBT thus possesses the necessary sensitivity for fluorescence imaging, as well as penetration and accurate positioning for MR imaging.

To test whether Gd-GFP³⁶⁺-dLBT can be used for tumor imaging, tumor-bearing mice received Gd-GFP³⁶⁺-dLBT via tail vein injection. Fluorescence and T₁-weighted MR images were

recorded to assess the distribution of Gd-GFP³⁶⁺-dLBT. Both measurements showed enhanced signals in the tumor after injection of Gd-GFP³⁶⁺-dLBT (Figure 3C, 3D). The time-dependent increase of contrast enhancement indicates accumulation of the protein in the tumor (Figure 3E). In addition, fluorescence imaging also showed the increased accumulation of the probe in tumor based on the *ex vivo* measurements in different time after the injection (Figure 3F). Taken together these results suggest that Gd-GFP³⁶⁺-dLBT is indeed useful for *in vivo* imaging.

To further investigate the biodistribution of the Gd-GFP³⁶⁺-dLBT probe, organs were collected 0.25, 0.5, 1, 3, and 6 hours post-injection for the *ex vivo* fluorescence imaging (Figure 3F). Significant amount of the protein was observed in liver 15 min after the injection, indicating rapid uptake of the probe by liver.²⁷ This is in agreement with the literatures that cationic probes are preferentially captured by the liver.^{28, 29} The fluorescence clearly decreased in liver after 30 min, and reached to the background level by 3 hours. The postponed accumulation and reduction were observed in intestine. This result suggests the quick hepatic clearance of the protein. In addition, the strong fluorescence signal was also observed in the kidney, peaking at 0.5-1 h post-injection and decreased during 6 h, indicating a relatively slower renal clearance. MR contrast enhancement in kidney and liver was also observed (Figure S8, S9). The lung showed a little protein accumulation, which was removed after 1 h. No fluorescence signal was observed in heart and spleen. Although the hepatic and renal clearance occurred, the increased accumulation of Gd-GFP³⁶⁺-dLBT is still observed in tumor during 6 h measurements, possibly due to the enhanced permeability and retention effect in solid tumors.⁴ The altered vasculature and lymphatic drainage allow accumulation of macromolecules in the tumor, resulting in passive targeting of Gd-GFP³⁶⁺-dLBT to the tumor.

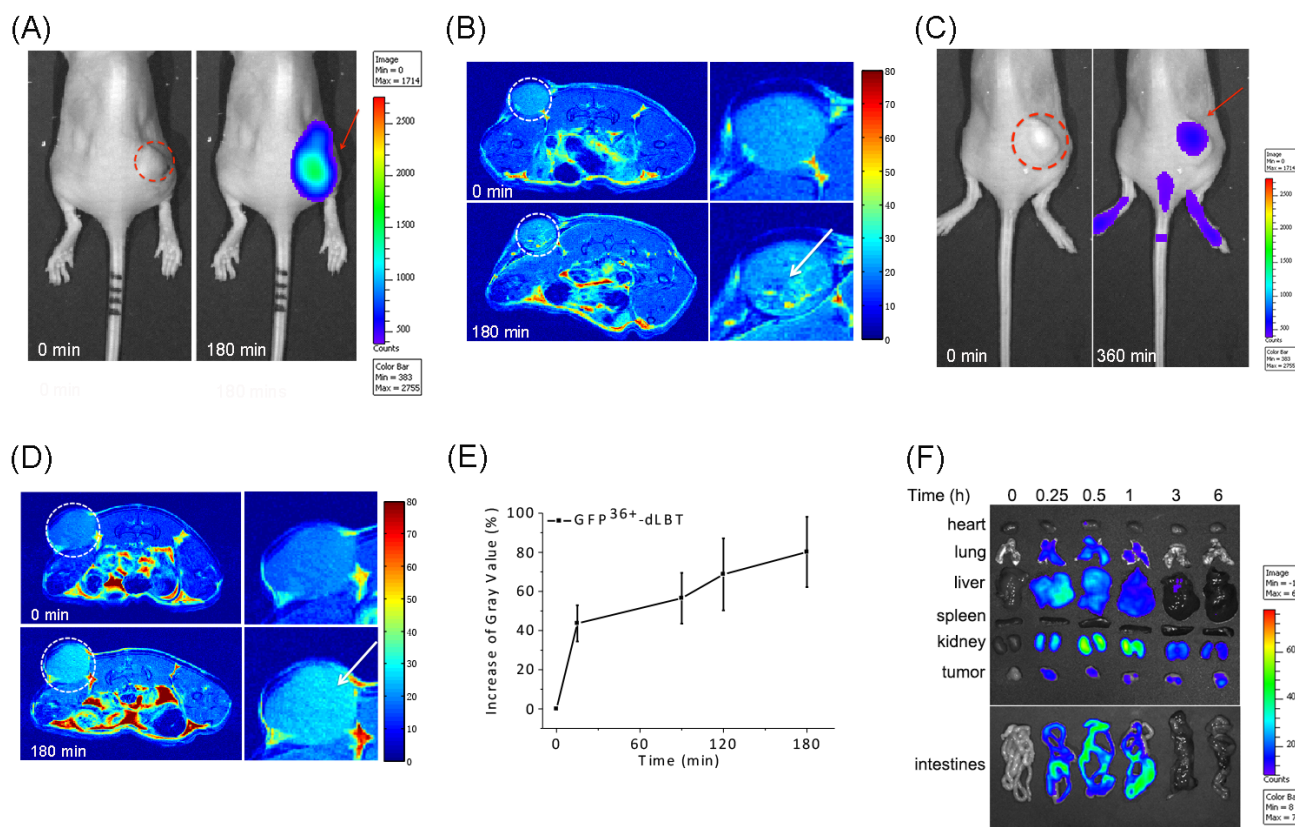


Figure 3. *In vivo* imaging of Gd-GFP³⁶⁺-dLBT. Dotted circles indicate the tumor site and arrows indicate the enhanced fluorescence signal or MR contrast. (A) Fluorescence imaging of nude mice bearing HepG2 tumors before (left) and after (right) intratumoral injection of Gd-GFP³⁶⁺-dLBT at a dose of 7.5 mg/kg. (B) T1-weighted MR images of tumor sites before and 3 h after intratumoral injection with Gd-GFP³⁶⁺-dLBT. The enlarged figures of the tumor site are shown on the right side. (C) Fluorescence imaging of tumor before (left) and 6 h after (right) tail vein injection with Gd-GFP³⁶⁺-dLBT (7.5 mg/kg). (D) T1-weighted MR images of tumor before (upper) and 3 h after (bottom) tail vein injection with Gd-GFP³⁶⁺-dLBT. (E) Quantitative analysis of tumor MR images at various times. The intensity of MR images was determined by standard region-of-interest measurement with Image J. Error bars denote standard deviation. (F) *Ex vivo* fluorescence imaging of the collected organs and tumor from the HepG2 xenograft nude mice at various time (0, 0.25, 0.5, 1, 3 and 6 h) after tail vein injection of the imaging probe.

The application of protein probes for multi-modal imaging has distinct advantages over chemically synthesized agents: 1) The preparation is straightforward and usually efficient. Routine protein expression and purification suffice to obtain the probes. 2) A tandem array of protein domains can be used to avoid interference of each functional modality, such as fluorescence quenching. 3) The function of a protein-based probe can be easily modified or further improved by adding/changing functional protein domains through standard protein engineering methods, for instance by fusion of an antibody to achieve specific targeting.^{30, 31} Protein-based MRI contrast agents have been made in exactly this manner.³² The use of bimodal imaging has been used to monitor tumor progression and therapeutic response.³³ Cells transfected with the gene of

supercharged GFP demonstrate bimodal optical imaging and an improved CEST MRI contrast in comparison to the wild type GFP.³⁴

The cellular delivery of MRI agents is considered an important approach for further development of contrast agents, as most currently used contrast agents are restricted to extracellular space.³⁵ Cellular imaging agents might find application in monitoring cancer metastases and in guiding surgery for tumor removal.³⁶ The ability to follow the metastatic process by tracking these intracellularly labeled cells at different cancer stage will provide a powerful tool for studying the mechanism of the metastasis and tumor dormancy. In addition, intracellular magnetic labeling technique has potential application in screening antimetastasis

Gadolinium measurement

10 μl Gd-DTPA or Gd-GFP³⁶⁺-dLBT was digested in concentrated HNO₃ for 12h and then the sample was diluted to 3 mL ultrapure water. The amount of Gd (III) was determined by ICP-MS.

In vitro relaxivity measurement

The MRI contrast was evaluated on a GE 1.5 T clinical MRI scanner. An array of microcentrifuge tubes containing different concentrations of the Gd-GFP³⁶⁺-dLBT and Gd-DTPA were prepared for MR imaging. Phantom images were acquired with an inversion recovery turbo spin echo pulse sequence with a repetition time (TR) of 300 ms and an echo time (TE) of 14 ms. Relaxivity values (r_1) were calculated from equation $r_1 = 1/T_{1s} - 1/T_{1c}$, where C is the concentration of contrast agent in mM (the measured Gd³⁺ concentrations by ICP-MS). T_{1s} is relaxation time with contrast agent and T_{1c} is relaxation time without contrast agent.

Cell culture and uptake

The human Henrietta Lacks cells (HeLa) and adenocarcinomic human alveolar basal epithelial cells (A549) were incubated at 37°C in 5% CO₂. Cells were incubated with different concentrations of GFP³⁶⁺-dLBT or Gd-GFP³⁶⁺-dLBT for 4 hours. Cells were washed five times to remove free gadolinium ions. The uptake was measured by a flow cytometer (BD FACSCalibur™).

Confocal fluorescence microscopy

Uptake of Gd-GFP³⁶⁺-dLBT was analyzed by confocal microscopy. HepG2 cells were grown on coverslips placed at the bottom of wells in a tissue culture plate. After incubation, the coverslips were mounted on slides using a media containing DAPI and sealed. Imaging was performed on a Zeiss LSM 710 laser confocal scanning microscope with a 100 \times objective lens.

Determination of Gd³⁺ content in cells

The HeLa and HepG2 cells were incubated with different concentrations of Gd-GFP³⁶⁺-dLBT or Gd-DTPA for 4 hours. Then the cells were trypsinized and washed several times before resuspension in PBS. The cells were adjusted to 2×10^6 cells/mL and then centrifuged at 3000 rpm for 15 min. The resulting cell pellets were digested in concentrated HNO₃ overnight and diluted to 4 ml in ultrapure water for ICP-MS measurement.

T₁-weighted MR imaging

The cell suspension was acquired in the same way as described above for the ICP-MS test. T₁-weighted images of the cell suspension were obtained on a 1.5 T clinical MR scanner. Phantom images were acquired with an inversion recovery turbo spin echo pulse sequence. The sequence used a repetition time (TR) of 300 ms and an echo time (TE) of 14 ms.

Animals

Nude mice harboring HepG2 tumors were used for FI and MRI experiments. All animal experiments were performed in compliance with institutional guidelines. The procedures were approved by the Animal Care and Use Committee of University of Science and Technology of China. To generate a tumor-bearing mouse model, the human hepatic carcinoma (HepG2) tumors were induced into 5 week old female nude mice by subcutaneous injection of 2.0×10^6 HepG2 cells. After the tumor grew to an appropriate size, the imaging probe was injected into the mice. Then the mice were anesthetized with an isoflurane gas mixture and positioned in the scanner for measurements.

In vivo fluorescence imaging

Image acquisition was performed on a Xenogen IVIS Lumina system (Caliper Life Sciences, Hopkinton, MA, USA). Data were analyzed using Living Image 3.1 software (Caliper Life Sciences). The mice injected with Gd-GFP³⁶⁺-dLBT were placed onto the warmed stage inside the IVIS Lumina light chamber and anesthesia was maintained with 2.5% isoflurane.

In vivo MRI

The MRI imaging was recorded on HepG2 tumor-xenografted nude mice after the injection of Gd-GFP³⁶⁺-dLBT for different time. The images were acquired on a 9 T MR scanner. The intensity of MR signal was analyzed using the software Image J.

Ex vivo analysis

Animals were sacrificed after contrast agent administration. Then major organs and tumors were dissected and collected for fluorescence scanning. Fluorescence images of major organs including brain, heart, liver, spleen, kidney, lung, intestines and tumors were obtained with a Xenogen IVIS Lumina system. Data were analyzed using Living Image 3.1 software.

Acknowledgements

We thank Professor Hidde L. Ploegh (Whitehead Institute, MIT, USA.) for critical reading of the manuscript and valuable comments. This work was supported by the National Science

Foundation of China (U1332210, 21171156), the National Basic Research Program of China (973 Program, 2012CB932502) and Collaborative Innovation Center of Suzhou Nano Science and Technology.

Notes and references

1. I. Y. Chen and J. C. Wu, *Circulation*, 2011, **123**, 425-443.
2. A. Hellebust and R. Richards-Kortum, *Nanomedicine*, 2012, **7**, 429-445.
3. A. Y. Louie, *Chem. Rev.*, 2010, **110**, 3146-3195.
4. E. K. Chow and D. Ho, *Sci. Transl. Med.*, 2013, **5**, 216rv214.
5. Z. L. Cheng, A. Al Zaki, J. Z. Hui, V. R. Muzykantov and A. Tsourkas, *Science*, 2012, **338**, 903-910.
6. E. S. Olson, T. Jiang, T. A. Aguilera, Q. T. Nguyen, L. G. Ellies, M. Scadeng and R. Y. Tsien, *Proc. Natl. Acad. Sci.*, 2010, **107**, 4311-4316.
7. D. Koktysh, V. Bright and W. Pham, *Nanotechnology*, 2011, **22**, 275606.
8. P. Verwilst, S. Park, B. Yoon and J. S. Kim, *Chem. Soc. Rev.*, 2015, **44**, 1791-1806.
9. E. Debroye and T. N. Parac-Vogt, *Chem. Soc. Rev.*, 2014, **43**, 8178-8192.
10. D. E. Lee, H. Koo, I. C. Sun, J. H. Ryu, K. Kim and I. C. Kwon, *Chem. Soc. Rev.*, 2012, **41**, 2656-2672.
11. J. H. Lee, Y. W. Jun, S. I. Yeon, J. S. Shin and J. Cheon, *Angew. Chem.*, 2006, **45**, 8160-8162.
12. J. Liu, K. Li, J. L. Geng, L. Zhou, P. Chandrasekharan, C. T. Yang and B. Liu, *Polym. Chem.* 2013, **4**, 1517-1524.
13. S. A. Corr, Y. P. Rakovich and Y. K. Gun'ko, *Nanoscale Res. Lett.*, 2008, **3**, 87-104.
14. J. M. Perez, T. O'Loughin, F. J. Simeone, R. Weissleder and L. J. Am. Chem. Soc., 2002, **124**, 2856-2857.
15. B. Dubertret, M. Calame and A. J. Libchaber, *Nat. Biotechnol.*, 2001, **19**, 680-681.
16. S. Li, J. Jiang, J. Zou, J. Qiao, S. Xue, L. Wei, R. Long, L. Wang, A. Castiblanco, N. White, J. Ngo, H. Mao, Z. R. Liu and J. J. Yang, *J. Inorg. Biochem.*, 2012, **107**, 111-118.
17. H. Korkusuz, K. Ulbrich, K. Welzel, V. Koeberle, W. Watcharin, U. Bahr, V. Chernikov, T. Knobloch, S. Petersen, F. Huebner, H. Ackermann, S. Gelperina, W. Kromen, R. Hammerstingl, J. Hauptenthal, F. Gruenwald, J. Fiehler, S. Zeuzem, J. Kreuter, T. J. Vogl and A. Piiper, *Mol. Imaging Biol.*, 2013, **15**, 148-154.
18. Z. Zhao, H. Fan, G. Zhou, H. Bai, H. Liang, R. Wang, X. Zhang and W. Tan, *J. Am. Chem. Soc.*, 2014, **136**, 11220-11223.
19. M. S. Lawrence, K. J. Phillips and D. R. Liu, *J. Am. Chem. Soc.*, 2007, **129**, 10110.
20. B. R. McNaughton, J. J. Cronican, D. B. Thompson and D. R. Liu, *Proc. Natl. Acad. Sci.*, 2009, **106**, 6111-6116.
21. L. J. Martin, M. J. Hahnke, M. Nitz, J. Wohnert, N. R. Silvaggi, K. N. Allen, H. Schwalbe and B. Imperiali, *J. Am. Chem. Soc.*, 2007, **129**, 7106-7113.
22. K. D. Daughtry, L. J. Martin, A. Sarraju, B. Imperiali and K. N. Allen, *ChemBiochem.*, 2012, **13**, 2567-2574.
23. D. B. Thompson, J. J. Cronican and D. R. Liu, *Method. Enzymol.*, 2012, **503**, 293-319.
24. S. H. Xue, J. J. Qiao, F. Pu, M. Cameron and J. J. Yang, *Wiley Interdisciplinary Rev. Nanomed. Nanobiotechnol.*, 2013, **5**, 163-179.
25. H. J. Weinmann, R. C. Brasch, W. R. Press and G. E. Wesbey, *AJR. Am. J. Roentgenol.*, 1984, **142**, 619-624.
26. Y. Wang, S. Song, J. Liu, D. Liu and H. Zhang, *Angew. Chem. Int. Ed.*, 2014, **54**, 536.
27. M. Yu and J. Zheng, *Nano Lett.*, 2015, **10**, 1021.
28. H. J. Lee and W. M. Pardridge, *Bioconjugate Chem.*, 2001, **12**, 995-999.
29. M. Longmire, P. L. Choyke and H. Kobayashi, *Nanomedicine*, 2008, **3**, 703-717.
30. O. Ziv, R. R. Avtalion and S. Margel, *J. Biomed. Mater. Res. A*, 2008, **85**, 1011-1021.
31. J. J. Qiao, S. Y. Li, L. X. Wei, J. Jiang, R. Long, H. Mao, L. Wei, L. Y. Wang, H. Yang, H. E. Grossniklaus, Z. R. Liu and J. J. Yang, *PLoS One*, 2011, **6**.
32. D. Grum, S. Franke, O. Kraff, D. Heider, A. Schramm, D. Hoffmann and P. Bayer, *PLoS One*, 2013, **8**, e65346.
33. A. Bhattacharya, S. G. Turowski, I. D. San Martin, A. Rajput, Y. M. Rustum, R. M. Hoffman and M. Seshadri, *Anticancer Res.*, 2011, **31**, 387-393.
34. A. Bar-Shir, Y. J. Liang, K. W. Y. Chan, A. A. Gilad and J. W. M. Bulte, *Chem. Commun.*, 2015, **51**, 4869-4871.
35. M. J. Allen, K. W. MacRenaris, P. N. Venkatasubramanian and T. J. Meade, *Chem. Biol.*, 2004, **11**, 301-307.
36. Q. T. Nguyen, E. S. Olson, T. A. Aguilera, T. Jiang, M. Scadeng, L. G. Ellies and R. Y. Tsien, *Proc. Natl. Acad. Sci.*, 2010, **107**, 4317-4322.
37. C. Heyn, J. A. Ronald, S. S. Ramadan, J. A. Snir, A. M. Barry, L. T. MacKenzie, D. J. Mikulis, D. Palmieri, J. L. Bronder, P. S. Steeg, T. Yoneda, I. C. MacDonald, A. F. Chambers, B. K. Rutt and P. J. Foster, *Magn. Reson. Med.*, 2006, **56**, 1001-1010.
38. L. Josephson, C. H. Tung, A. Moore and R. Weissleder, *Bioconjugate Chem.*, 1999, **10**, 186-191.
39. V. Economopoulos, Y. H. Chen, C. McFadden and P. J. Foster, *Transl. Oncol.*, 2013, **6**, 347-354.
40. M. Lewin, N. Carlesso, C. H. Tung, X. W. Tang, D. Cory, D. T. Scadden and R. Weissleder, *Nat. Biotechnol.* 2000, **18**, 410-414.
41. T. Yamane, K. Hanaoka, Y. Muramatsu, K. Tamura, Y. Adachi, Y. Miyashita, Y. Hirata and T. Nagano, *Bioconjugate Chem.*, 2011, **22**, 2227-2236.